

A comparison of fictitious domain methods appropriate for spectral/*hp* element discretisations

P.E.J. Vos ^{*}, R. van Loon, S.J. Sherwin

Department of Aeronautics, Imperial College London, South Kensington Campus, SW7 2AZ London, UK

Received 7 September 2007; received in revised form 28 October 2007; accepted 29 November 2007

Available online 10 January 2008

Abstract

The fictitious domain, finite cell and fat boundary method, which are commonly adopted for fluid–structure interaction (FSI) problems, have been considered and implemented in a spectral/*hp* element code for a 1D test problem. The finite cell and fat boundary method are extended for the general case of a deformable solid in a fluid, and analysed. Furthermore, a new implicit variation of the fat boundary method is proposed. The 1D framework allows for a clear and detailed analysis of the different approaches and to highlight the similarities and differences between the methods. Exponential *p*-convergence, which is typical for smooth solutions discretised with spectral/*hp* elements, is demonstrated for all methods except the classic fictitious domain formulation. This overview can be considered as a starting point to study the capability, advantages and disadvantages of these methods for fluid–structure interaction problems in a more realistic setting and in higher dimensions.

© 2007 Elsevier B.V. All rights reserved.

Keywords: Fluid–structure interaction; Fictitious domains; Finite cell method; Fat boundary method; Spectral/*hp* element method; Lagrange multipliers

1. Introduction

Many methods have been introduced for fluid–structure problems that consider non-matching overlapping meshes such as the immersed boundary method [16,7], immersed continuum method [18], immersed finite element method [21], immersed interface method [13], fat boundary method [14,3] or fictitious domain method [10,1,20]. All approaches are closely related and a general problem definition can be formulated as a solid body (rigid or deformable) embedded in a fluid domain. The object can either define the boundary of the fluid domain, an obstruction in the flow or a freely moving body in the flow. To capture the interaction between the solid and the fluid kinematic and dynamic constraints have to be imposed on both domains. The main difference between the afore-mentioned methods is how these constraints are enforced in the different numerical frameworks.

The main motivation to use overlapping approaches is to apply a structured background mesh (grid) that will not depend on the complexity of the geometry of the obstacle or its motion. In particular for unsteady calculations it is advantageous that the global mesh does not require updating, which can be a time-consuming and difficult task. As a consequence the global matrix arising from the discretisation of the PDE will remain the same throughout the computation and therefore have to be computed only once. Furthermore, when a partitioned solution scheme is applied with separate solves for the fluid, structure and/or interface, the structured fluid grids allow for efficient solution procedures. Although many methods have been proposed in a finite element, finite difference or finite volume context only few publications exist on the performance of non-matching approaches for high-order discretisations such as the spectral/*hp* element method. Therefore we would like to highlight this part of the literature by exploring various overlapping approaches in the context of the spectral/*hp* element method. A central issue in this discussion will be whether these approaches could

^{*} Corresponding author. Tel.: +44 (0)20 75945103.

E-mail address: peter.vos@imperial.ac.uk (P.E.J. Vos).

fully benefit from the exponential p -convergence, typical for spectral/ hp methods [12].

A first approach that uses spectral/ hp elements to describe the interaction of a non-matching object arises from the field of solid mechanics and was named the finite cell method [15]. Although the method does not consider overlapping meshes it clearly illustrates some of the issues that are typical for overlapping methods. In their work Parvizian et al. [15] propose a method to compute solids with randomly shaped voids on a regular grid using spectral/ hp elements. The formulation allows for jumps of the material coefficient from unequal to zero across the material to zero in the void. For the classical problem of a circular void in a plate exponential p -convergence is demonstrated.

The fictitious domain method as exploited by Glowinski et al. [10] in a finite element code has been explored for a spectral/ hp framework by Dong et al. [6]. A distributed Lagrange multiplier was used to couple the object to the underlying fluid. Exponential p -convergence was demonstrated for a fictitious domain approach with overlapping fluid domains and further performance was tested using the exact solution for a Wannier flow (Stokes flow) and using the flow around a cylinder (Navier-Stokes).

Another method we would like to address here is the fat boundary method proposed by Maury [14], in which a void is enveloped with a nicely aligned fluid layer that overlaps the global fluid domain. The method originates from the area of domain decomposition and reminds of chimera methods, that have been introduced to improve the accuracy in the vicinity of a structure. Both domains are solved separately in a fixed point iterative scheme. Although an error estimate was defined for any order of P [3], only h -convergence was demonstrated for multiple particles in a fluid domain using linear finite elements.

Inspired by comparison studies like [18,5,17] our aim is to explore non-matching, overlapping approaches that can be used with spectral/ hp element methods and highlight the (dis)advantages. It was chosen to adopt methods from literature that were proposed in a finite or spectral/ hp element framework. Therefore we chose the finite cell method [15], the fictitious domain method [10,6,20] and fat boundary method [14] that have been implemented in a 1D spectral/ hp element framework. Based on e.g. [4], it can be appreciated that such a 1D analysis allows for a better insight in the underlying mechanisms of the different methods. Furthermore, we extend the finite cell and fat boundary method that were both formulated for problems characterised by a void, in order to deal with a broader range of problems. In addition, an implicit variation to the fat boundary method is proposed with the use of Lagrange multipliers. The paper is organised as follows: Section 2 is used to introduce the governing equations and to give the analytical solution for our test problem along with some general remarks regarding the solution domain(s). In Sections 3–5 the finite cell method, fictitious domain method and fat boundary method are explained in

some detail and evaluated in terms of p -convergence. Our variation of the fat boundary method is proposed in Section 6 and finally, in Section 7 all results and their implications for 2D and 3D implementations will be discussed.

2. Test problem: a 1D fluid with an immersed solid

First, a test problem is defined that will be used to facilitate a comparison of the individual approaches. Consider a one-dimensional domain $\Omega_g = [0, L]$, which is characterised by two interfaces that are located at A and B, respectively, as depicted in Fig. 1. The interfaces divide the global domain into two different physical parts: the domain enclosed by the interfaces, which will be denoted as $\Omega_s = [A, B]$, and the remaining part $\Omega_f = \Omega_g \setminus \Omega_s = [0, A] \cup [B, L]$.

Possible physical interpretations for the enclosed domain are: a void inside a solid (e.g. a perforated plate), a rigid particle or a solid immersed in a flow. In this work, we will mainly adopt the last interpretation. More specifically, we will focus on solutions of the problem:

Find u_f and u_s which solve the following set of Poisson equations,

$$\frac{d}{dx} \left(\theta_f \frac{du_f}{dx} \right) = f_f \quad \text{on } \Omega_f \quad (1)$$

$$\frac{d}{dx} \left(\theta_s \frac{du_s}{dx} \right) = f_s \quad \text{on } \Omega_s \quad (2)$$

subject to the constraints,

$$u_f = u_s \quad \text{on } \partial\Omega_s \equiv A, B \quad (3)$$

$$\theta_f \frac{du_f}{dx} = \theta_s \frac{du_s}{dx} \quad \text{on } \partial\Omega_s. \quad (4)$$

As this can be considered as a simplified 1D fluid–structure interaction problem of a flexible body (the solid) embedded in a flow (the fluid), we will use the subscripts s and f accordingly throughout this work. In this context, Eq. (3) represents a no-slip condition between fluid and solid, while Eq. (4) ensures force-equilibrium at the interfaces. Although the flexible body will not deform or move through the domain because a steady problem is considered, the phrase ‘flexible body’ is merely used to emphasise that the solid is described by a PDE of which the (non-homogeneous) solution is a priori unknown.

Clearly, continuity of the solution is enforced by condition Eq. (3). However, in general, the fluid and solid will be described by a different diffusion coefficient θ and forcing function f in the governing equations Eqs. (1) and (2). As a consequence, the exact solution will be characterised by a jump in the first derivative (resulting from condition Eq. (4)) and a discontinuous second derivative respectively,

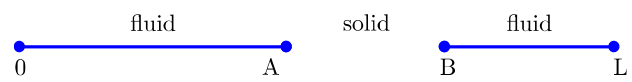


Fig. 1. Problem description: a 1D model of a solid immersed in a fluid.

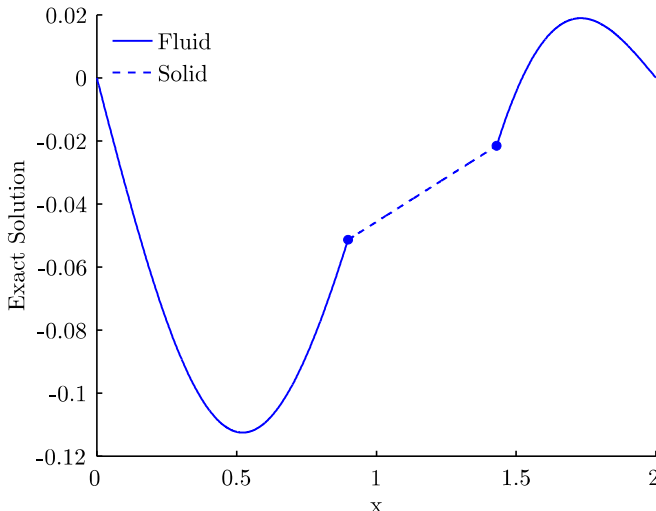


Fig. 2. The exact solution for the 1D fluid–structure interaction test problem.

both located at the interface-points A and B. These discontinuities will be of great influence when studying the different fluid–structure interaction approaches in a spectral/ hp framework, in particular with respect to the error convergence.

When studying problems with a void on Ω_s rather than an immersed solid, the problem will be governed solely by Eq. (1) supplied with either Dirichlet or Neumann boundary conditions at the interfaces A and B.

For the numerical model, we will take $\theta_f = 1$, $\theta_s = 5$, $f_f = \sin(\pi x)$, $f_s = 0$, $A = \frac{71}{79}$, $B = \frac{113}{79}$, $L = 2$. The exact solution for this choice of parameters, together with homogeneous Dirichlet boundary conditions at the outer bounds, is shown in Fig. 2.

In the subsequent sections, error calculations will be performed to compare the different methods. Throughout this work, for any approximation u_{app} on an interval $[a, b]$, we will consider the L_2 error ϵ normalised by the length of the interval, defined by

$$\epsilon = \sqrt{\frac{\int_a^b (u_{\text{ex}} - u_{\text{app}})^2 dx}{(b - a)}} \quad (5)$$

in which u_{ex} is the exact solution.

3. The fictitious domain method

In the fictitious domain (FictD) method, which has been extensively studied in for example [8–10,20], the fluid solution is continuously extended into the interior of the solid domain. At the discrete level, this allows the use of structured, non-boundary fitted meshes. As a result, the support of the fluid solution u_f will then correspond to the global domain Ω_g as opposed to the physical fluid domain Ω_f . For clarity, this globally defined fluid will be denoted as u_g , where the subscript g refers to global. Although it is obvious that u_g should describe the fluid solution in the

fluid part of the domain, u_g may be arbitrary inside Ω_s , as it does not describe part of the physical solution.

Although the idea of an extended domain is employed in a variety of methods, the term fictitious domain methods is, in the literature, mainly used for those methods combining overlapping domains in a finite element framework, together with Lagrange multipliers to enforce the coupling constraints. To introduce further details, we will first elaborate on the existing FictD method in the context of our one-dimensional test problem of Section 2. After this, the FictD method will be considered with a spectral/ hp element spatial discretisation.

3.1. The fictitious domain method for fluid–structure interaction problems

As mentioned earlier, it is typical for fictitious domain methods that the computational domain Ω_f is extended to the global domain Ω_g . This extension of Ω_f introduces the following issue: what should happen to u_g inside the fictitious part of the domain? Different options have been proposed in the literature. In [8] covering the FictD method for the Dirichlet problem, Glowinski chose to extend the governing fluid equation, Eq. (1), with a suitable extension of f_f into Ω_s . Considering our choice of parameters, possible extensions for f_f are: $f_f = \sin(\pi x)$ on Ω_s or the more straightforward choice $f_f = 0$ on Ω_s . Fig. 3 depicts the fictitious fluid solution for both choices. In this case, discrete Lagrange multipliers at the physical interfaces are employed to enforce the constraints Eqs. (3) and (4). Another option for the fictitious fluid has been suggested in the context of fluid–structure interaction problems. In [10,20], it has been proposed to enforce the solution of the fictitious fluid $u_g|_{\Omega_s}$ to equal the solid solution u_s . Due to our choice of parameters for the test problem, this happens to result in a solution similar to a homogeneous

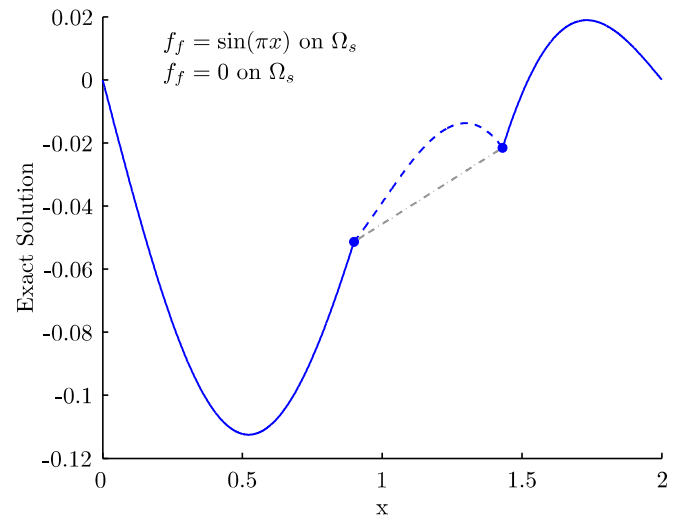


Fig. 3. Possible solutions of the fictitious fluid by extending the governing fluid equation inside the solid domain with a suitable extension of the forcing function f_f .

extension of f_f into Ω_s . Notice that in all cases the global solution u_g shows a kink at the physical interfaces, which corresponds to a jump in the first derivative.

Following this latter approach, the no-slip constraint, Eq. (3), will be extended and replaced by the constraint,

$$u_f = u_s \quad \text{on} \quad \Omega_s. \quad (6)$$

In the FictD method, a distributed Lagrange multiplier $\lambda(x)$, defined over the entire domain Ω_s , is employed to enforce this new constraint. In his work [20], Yu derived a weak distributed Lagrange multiplier/fictitious domain (DLM/FictD) formulation for those FSI problems in which the solid body is governed by a PDE. Applied to the 1D test problem of Section 2, the weak formulation is given by: find $\{u_f, u_s, \lambda\} \in H_0^1(\Omega_g) \times H^1(\Omega_s) \times \Lambda$ such that,

$$\int_0^L \theta_f \frac{du_g}{dx} \frac{dv_g}{dx} dx - \langle \lambda, v_g \rangle_{\Omega_s} = - \int_0^L f_f v_g dx \quad \forall v_g \in H_0^1(\Omega_g) \quad (7)$$

$$\begin{aligned} & - \int_A^B \theta_f \frac{du_g}{dx} \frac{dv_s}{dx} dx + \int_A^B \theta_s \frac{du_s}{dx} \frac{dv_s}{dx} dx + \langle \lambda, v_s \rangle_{\Omega_s} \\ & = - \int_A^B (f_s - f_f) v_s dx \quad \forall v_s \in H^1(\Omega_s) \end{aligned} \quad (8)$$

$$\langle u_g - u_s, \gamma \rangle_{\Omega_s} = 0 \quad \forall \gamma \in \Lambda, \quad (9)$$

where $\langle \cdot, \cdot \rangle_{\Omega_s}$ denotes the inner product corresponding to the Lagrange multiplier space Λ which will be defined in the following section.

We would like to emphasise that this version of FictD method is conceptually similar to the immersed continuum method as described by Wang [18]. In both methods, the fluid domain is extended to include the submerged solid and the fictitious part of the fluid is chosen to represent the solid solution on Ω_s . However, the two methods differ in the way they solve the problem. In the FictD method, the coupling term locally converting the fluid equation into the solid equation on Ω_s is represented by the distributed Lagrange multiplier $\lambda(x)$ as can be appreciated from Eq. (7). In the immersed continuum method, the coupling term is calculated explicitly using the solid equation and coupled back into the fluid equation employing appropriate interpolation methods. For more details, we refer the reader to [18,19,21]. Due to the similarities of the strong form, we believe both methods will exhibit a similar convergence behaviour in a spectral/ hp context and the results presented in the remainder of this section are also valid for the immersed continuum method.

3.2. Extension to higher order

The potential of the fictitious domain method has been shown in various works [10,2,11,20]. In order to solve the variational problem governed by Eqs. (7)–(9), the computational domains Ω_g and Ω_s are discretised using structured meshes, while the solution, in most cases, is sought after in the finite dimensional function spaces spanned by the

C^0 -continuous linear basis function of the finite element method.

A first extension of the fictitious domain method to the spectral/ hp element method has been discussed in the work of Dong et al. [6]. In this work, the same set of equations, Eqs. (7)–(9), are being solved with the only difference that the finite dimensional function spaces in which the solution is sought, are now spanned with the P th order polynomial expansion functions that are typical for the spectral/ hp element method [12]. Moreover, Dong enforces the distributed constraint, Eq. (6), via a penalty method. However, as this latter fact will not influence our discussion, we will maintain the enforcement through Eq. (9) in our formulation. For the implementation, we used $\Lambda = L^2(\Omega_s)$, such that at the discrete level, the Lagrange multiplier λ can be expanded as a set of Dirac delta functions at a set collocation points, in which the inner duct $\langle \cdot, \cdot \rangle_{\Omega_s}$ corresponds to the discrete L^2 inner product. Furthermore, for our test case, the global domain Ω_g is discretised in five equispaced elements, while the solid mesh consists of two equispaced elements.

The extension to the spectral/ hp element approach is inspired by the inherent properties of this high-order method. Namely, if sufficient smoothness of the exact solution can be guaranteed, the spectral/ hp element method is known to converge spectrally, i.e. the approximation error decreases exponentially as the order of polynomial order of the expansion increases. It is the fast exponential convergence rate and hence, accurate approximations, that makes the spectral/ hp element method a potentially attractive approach. In order to benefit from these properties, the fictitious domain method has been implemented in a spectral/ hp element framework.

In Fig. 4 showing the L_2 error of the numerical results plotted against the polynomial order for our 1D test problem, it can be seen that the desired exponential convergence rate is absent. This unfavourable convergence rate in a

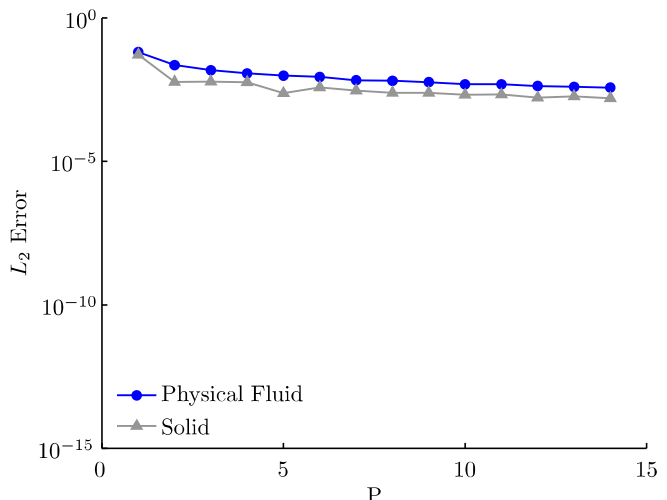


Fig. 4. p -Convergence of the high-order fictitious domain method applied to the 1D FSI test problem.

spectral/ hp context can be explained by the shape of the exact solution. As discussed in Section 3.1, the global solution u_g exhibits irregularities at the physical interfaces, which severely limits its smoothness. It can be appreciated that a spectral/ hp element approximation that uses C^0 connected polynomials to approximate the solution, cannot be employed to properly model kinks in the interior of an element. This lack of smoothness of u_g , a necessary condition for high-order approximations, therefore destroys the exponential convergence.

Note that this loss of spectral error-convergence is not limited to the distributed Lagrange multiplier/fictitious domain method. Also in the case of discrete Lagrange multipliers that are only imposed on the solid boundary, similar behaviour will be observed. As shown in Fig. 3, the exact solution will ‘suffer’ from similar kinks at the physical interfaces, which will result in a comparable convergence rate of the error. In summary, a spectral/ hp element implementation of the fictitious domain methods covered in this section will not maintain the high-order advantages that are common for the spectral/ hp element method.

Finally, it can be deduced that optimal error-convergence will arise in two cases. First, if the global fluid mesh happens to align with the physical interfaces, the irregularities of u_g are located at grid points of the global mesh. Because a general spectral/ hp element approximation is only C^0 continuous at the element boundaries, and the jump at the interface neatly fits into the formulation, the approximation spectral/ hp element will allow for such a jump and consequently, exponential error-convergence will be regained. However, as fictitious domains methods are mainly employed to allow the use of non-matching grids, this is a fairly trivial case. Secondly, if the exact solution does not exhibit irregularities, e.g. in the (again trivial) case of a fluid embedded in a fluid (both described by the same parameters θ and f), there will be exponential convergence as well. Dong et al. [6] demonstrated this convergence for a two-dimensional test problem.

4. The finite cell method

Recently, Parvizian et al. [15], adopted the spectral/ hp element method in combination with non-boundary fitted meshes. Their method, referred to as finite cell method (FCM), converges exponentially for applications in linear elasticity. More specifically, in their analysis, they focus on solids with randomly shaped stress-free voids. Mathematically, this stress-free void imposes homogeneous Neumann boundary conditions on the solid at the solid–void interface.

4.1. The finite cell method for Neumann problems

With respect to our one-dimensional test problem, this Neumann problem is governed by Eq. (1) supplied with Neumann boundary conditions $\frac{du_f}{dx} = g_A$, $\frac{du_f}{dx} = g_B$ at the points A and B, respectively. For generality, we will study

the case of non-homogeneous Neumann boundary conditions. Analogue to the fictitious domain methods, the finite cell method extends the computational domain beyond the physical domain to include the global domain Ω_g . So far, with respect to the choice of computational domains and the corresponding interface-independent structured meshes, the finite cell method is similar to the fictitious domain method. The methods are different in the way they extend the governing equation, Eq. (1), inside the fictitious region Ω_s . While the fictitious domain method simply solves the governing equation inside the fictitious part of the global domain for a given suitable extension of the forcing function f_f (see Section 3.1), the finite cell method follows another approach. In the finite cell method, the governing equation is still solved in the fictitious part of the global domain, but an extremely small value is chosen for the diffusion coefficient θ_f , while the forcing function is extended as $f_f = 0$. In a linear elasticity context, this corresponds to filling the void with a very soft material on which no body forces are applied. As this fictitious soft material can be understood to absorb only little energy, there will be minimal interference with the solution of the physical material. In a weak form, this new problem can be formulated as: find $u_g \in H_0^1(\Omega_g)$ such that,

$$\int_0^L \theta \frac{du_g}{dx} \frac{dv_g}{dx} dx = - \int_0^L f_f v_g dx - g_A v_g(A) + g_B v_g(B) \quad \forall v_g \in H_0^1(\Omega_g) \quad (10)$$

with $\theta = \theta_f$ for $x \in \Omega_f$ and $\theta \ll 1$ for $x \in \Omega_s = [A, B]$. Notice that for a value of $\theta \neq 0$ on Ω_s , there is no strict equivalency between the solution of the original problem, prescribed by Eq. (1), and the solution of the modified problem in the weak form, given by Eq. (10). That is why, ideally, one would like to use a value of $\theta = 0$ on the fictitious domain, which would make both problems equivalent. However, in the context of an extended computational domain, the choice of $\theta = 0$ is not an option, as this implies that the solution u_g is not described on the fictitious domain. Although this is irrelevant and leads to an ill-posed problem on continuous level, it does make sense on a discrete level for some cases. With this in mind, Parvizian and co-workers proposed following approach for the discretised global computational domain Ω_g :

- For these elements of Ω_g entirely embedded in the fluid: take $\theta = \theta_f$.
- For these elements of Ω_g entirely embedded in the solid: take $\theta \ll 1$.
- For these elements of Ω_g intersected by the fluid–solid interface: take $\theta = \theta_f$ for $x \in \Omega_f$, $\theta = 0$ for $x \in \Omega_s$.

To appreciate why a value of $\theta = 0$ can be used for the elements intersected by the interface, consider the problem governed by Eq. (10), being discretised using spectral/ hp finite elements on a structured, interface-independent, grid. For our 1D test problem two spectral elements were

intersected by the interfaces A and B. Parvizian et al. [15] referred to these elements as finite cells. In those finite cells, the discretised equivalent of Eq. (10) should be evaluated on the elemental level before global assembly. Although the integrand will be partly zero for those finite cells, this discretised elemental set of equations will result in a solvable system. Because the fictitious part of the problem does not add weight to the integral, all degrees of freedom will be employed to approximate the solution in the physical part of the cell. As a result, the approximation, defined on the fictitious part of the finite cell, will in no way interfere or pollute the physical part of the approximation. As will be demonstrated later, it is this fact which will allow for exponential error-convergence. Furthermore, the fictitious part of the approximation does not converge to a specific solution and depends highly on the employed expansion order.

For the elements entirely embedded in the fictitious part of the domain, Eq. (10) cannot be solved for a value of $\theta = 0$, as it would read $0 = 0$. That is why for these elements, θ is chosen to be very small. Parvizian et al. [15] stated that any θ as small as 10^{-10} can be employed without affecting the numerical results.

In Fig. 5, the numerical results of the finite cell method applied to the 1D test problem with Neumann boundary conditions $g_A = g_B = 0.5$ are presented. It can be clearly observed that the FCM does converge exponentially for this case. A similar convergence rate was demonstrated by Parvizian et al. [15] for a two-dimensional perforated plate with zero-traction boundary conditions.

4.2. The Lagrange multiplier/finite cell method

Based on the observation that the finite cell method shows great similarity to the fictitious domain methods, in this section, we will introduce Lagrange multipliers in a finite cell method context. The combined method will

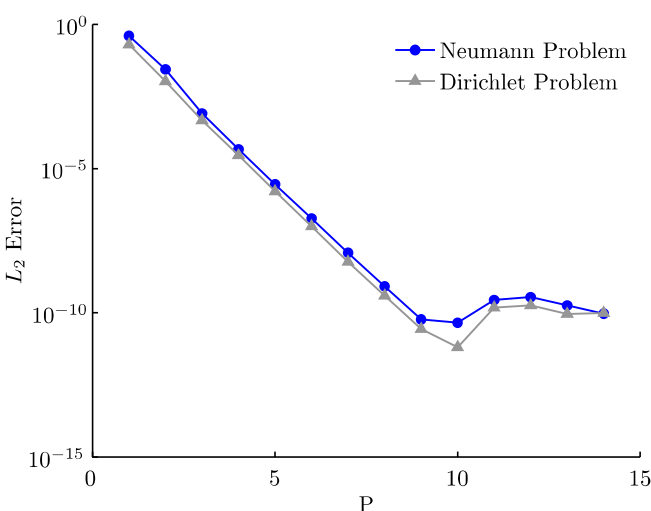


Fig. 5. Exponential p -convergence of the finite cell method applied to the 1D Dirichlet and Neumann test problem.

be referred to as the Lagrange multiplier/finite cell method (LM/FCM). This extension will allow us to deal with a broader range of problems using the finite cell method.

4.2.1. The LM/FCM for Dirichlet problems

Analogue to the FictD method for the Dirichlet problem [8], discrete Lagrange multipliers at the points A and B can be employed to impose the Dirichlet boundary conditions to solve the problem governed by Eq. (1) and supplied with Dirichlet boundary conditions at the inner boundaries. Except for the governing equation for u_g inside the fictitious part of the domain Ω_g , the FCM is completely similar to the FictD method for this problem. As a result, Lagrange multipliers can be introduced in a similar fashion as described in [8]. The error convergence of the spectral/ hp element approximation of this problem is depicted in Fig. 5 for the Dirichlet boundary conditions $g_A = 0$, $g_B = -0.06$. Exponential convergence is also observed for this case.

4.2.2. The LM/FCM for fluid–structure interaction problems

The same approach can be extended to fluid/flexible body interaction problems. As the finite cell method already determines the behaviour of the global solution u_g inside the fictitious part of the domain, two discrete Lagrange multipliers at both the interfaces A and B are sufficient to couple the fluid and the solid, at these points only. In this respect, the implementation differs from the fictitious domain method of Section 3.2, where a distributed Lagrange multiplier, coupling both objects on the entire domain Ω_s , was employed. For our 1D test problem as introduced in Section 2, the problem can be formulated in a weak form as

Find $\{u_f, u_s, \lambda_{A,B}\} \in H_0^1(\Omega_g) \times H^1(\Omega_s) \times \mathbb{R}$ such that,

$$\begin{aligned} & \int_0^L \theta \frac{du_g}{dx} \frac{dv_g}{dx} dx + \lambda_B v_g(B) - \lambda_A v_g(A) \\ &= - \int_0^L f_f v_g dx \quad \forall v_g \in H_0^1(\Omega_g) \end{aligned} \quad (11)$$

$$\begin{aligned} & \int_A^B \theta_s \frac{du_s}{dx} \frac{dv_s}{dx} dx - \int_A^B \theta \frac{du_g}{dx} \frac{dv_s}{dx} dx - \lambda_B v_s(B) + \lambda_A v_s(A) \\ &= - \int_A^B (f_s - f_f) v_s dx \quad \forall v_s \in H^1(\Omega_s) \end{aligned} \quad (12)$$

$$\gamma_A (u_g - u_s)|_{x=A} = 0 \quad \forall \gamma_A \in \mathbb{R} \quad (13)$$

$$\gamma_B (u_g - u_s)|_{x=B} = 0 \quad \forall \gamma_B \in \mathbb{R}. \quad (14)$$

In Fig. 6, we illustrate that the finite cell method properly approximates the exact solution of our test problem. Bear in mind that for the elements cut by the interfaces, the fictitious part of the solution is just the extension of the best, in a Galerkin sense, P th order polynomial approximation of the exact solution in the physical part of the finite cell. Fig. 7 shows the exponential error-convergence of the method. Although both the error of the fluid and the solid decay exponentially, notice the difference in convergence rate. The solid solution u_s converges considerably faster than the fluid solution u_g .

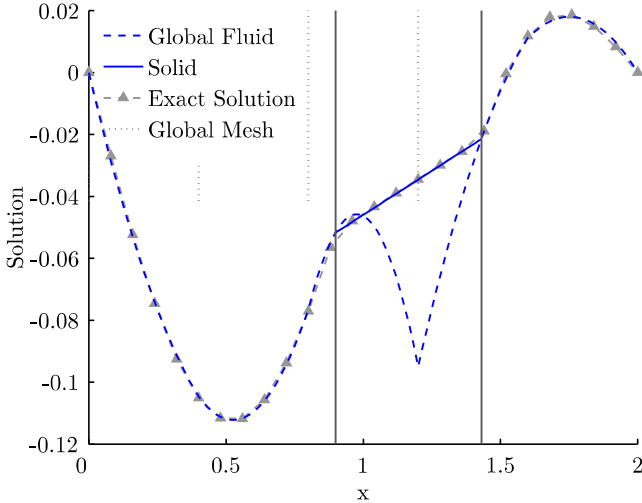


Fig. 6. The finite cell approximation of the 1D FSI test problem employing a spectral/ hp expansion with $P = 2$.

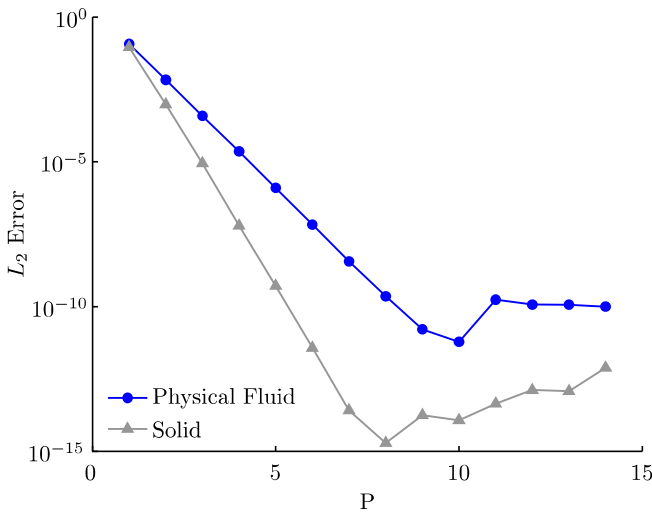


Fig. 7. Exponential p -convergence of the finite cell method applied to the 1D FSI test problem.

4.3. Discussion

4.3.1. Implementation issues

Despite the fact that it benefits from exponential convergence, the finite cell method is also characterised by some limitations. Although it exploits one of the advantages of a fixed structured mesh, i.e. no need to remesh when dealing with moving bodies, it does not fully benefit from it. Due to the choice to locally modify the governing global equation on the fictitious domain, the global matrix will vary in time and hence, need constant monitoring and updating. This will increase the cost of the method.

4.3.2. Extension to multiple dimensions

As mentioned afore, the calculation of the elemental stiffness matrix for the elements intersected by the physical interface, will involve the evaluation of an integral with dis-

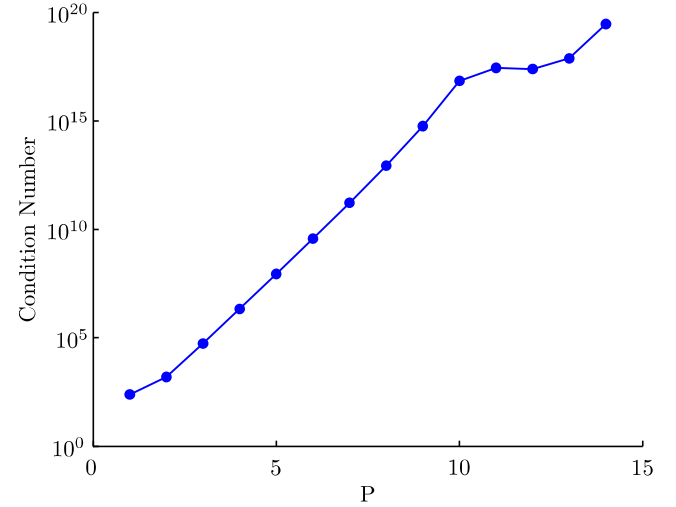


Fig. 8. The condition number of the resulting linear algebraic system when employing the finite cell method for the 1D FSI test problem plotted as a function of the polynomial order P .

continuous integrand, see Eq. (10). In 1D, it is straightforward to split up such integrals in order to avoid integration errors. This is the approach we followed to generate the numerical results presented above. However, when considering 2D or even 3D problems, exact evaluation of these integrals will be very complex, if not impossible. In their work, Parvizian et al. [15] adopted a high-order Gaussian quadrature approach with up to 100 integration points to approximate the integral. Despite their effort, they noticed a loss of exponential error convergence due to the integration errors induced.

4.3.3. Ill-posedness of the problem

Besides the exponential decay of the error, the condition number of the resulting algebraic system seems to increase exponentially with respect to the polynomial order, as depicted in Fig. 8 for the 1D FSI test problem. Similar behaviour can be observed for the other test problems studied in this section. This implies that for high polynomial order, the system becomes ill-posed. This might be appreciated as on continuous level, an ill-posed problem is being solved for the fluid variable u_g , see Section 4.1. It can also explain why in Fig. 7, the convergence rate and maximal accuracy is lower for the fluid than for the solid. It will appear that this fluid convergence rate and corresponding accuracy will be lower compared with the methods of following sections.

5. The fat boundary method

In [14], Maury proposed the fat boundary method (FBM) to solve the Poisson problem in a domain with one or multiple voids. The idea was to extend the computational domain underneath the hole, but despite this coarse background mesh, also to keep the capability of accurately approximating the solution in the neighbourhood

of the holes. Therefore, a 'halo' boundary domain was introduced around the void and referred to as a fat boundary. In this halo region, which is conformly attached to the void, a finer mesh can be employed which results in the desired resolution in the vicinity of the void.

5.1. The fat boundary method for fluid–structure interaction problems

To further introduce the fat boundary method, we will apply the approach to the 1D FSI test problem of Section 2. This extension to fluid–structure interaction problems is based on Maury's [14] formulation of the Poisson problem with non-homogeneous Dirichlet boundary conditions at the void. In this case, the halo boundary can be interpreted as a boundary layer mesh attached to the solid. A representation of the different computational domains is depicted in Fig. 9.

A new solution variable is introduced on the halo boundary. This variable represents the physical fluid on the halo domain. While generally, in multiple dimensions, the halo boundary consists of a single domain, two separated halo domains appear in our one-dimensional problem. Consequently, a solution variable is defined on each of the halos, and they will be referred to as halo fluid u_{h_1} and u_{h_2} , respectively.

Since the fat boundary method employs a global computational domain Ω_g that is partly fictitious, the issue of how to extend u_g into the solid domain also arises in this method. Similar as in the DLM/FictD methods discussed earlier, u_g is chosen to represent the solid solution in the fictitious part of its computational domain. However, due to the introduction of a halo mesh, the performance of the FBM will appear to differ from the DLM/FictD method, as demonstrated later in this section.

The fat boundary method is based on splitting the original problem into two local sub-problems. On one hand, the global fluid solution will be calculated on the global domain Ω_g , while on the other hand, the combined solid/halo fluid problem will be solved on their corresponding domains. Both problems will be solved in a fixed point iteration scheme, which can be summarised as a loop over the following steps:

1. Solve Problem 1: the global fluid problem.
2. Extract the values of the global fluid solution at points a and b and impose them as Dirichlet boundary conditions of Problem 2.
3. Solve Problem 2: the combined solid/halo fluid system.

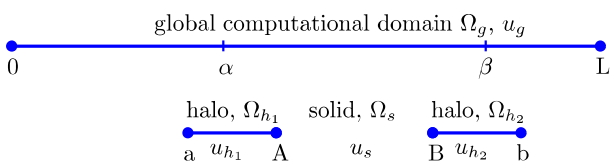


Fig. 9. The different computational domains of the fat boundary method applied to the 1D FSI test problem.

4. Extract the value of the derivatives of both the solid and halo fluid at the physical interfaces A and B. Impose this result as a singular source term in Problem 1 to obtain the correct jump in first derivative of u_g across the physical interfaces.

In strong form, this can be formulated as

Find $\{u_f, (u_{h_1}, u_s, u_{h_2})\} \in H_0^1(\Omega_g) \times V$ such that,

$$\begin{aligned} \text{Problem 1 : } & \begin{cases} \frac{d}{dx} \left(\theta_f \frac{du_{h_1}}{dx} \right) = f_f & \text{on } \Omega_{h_1} \\ \frac{d}{dx} \left(\theta_s \frac{du_s}{dx} \right) = f_s & \text{on } \Omega_s \\ \frac{d}{dx} \left(\theta_f \frac{du_{h_2}}{dx} \right) = f_f & \text{on } \Omega_{h_2} \\ u_{h_1}|_a &= u_g|_a \\ u_{h_2}|_b &= u_g|_b \end{cases} \\ \text{Problem 2 : } & \begin{cases} \frac{d}{dx} \left(\theta_f \frac{du_f}{dx} \right) = f_f + \theta_f \left(\frac{du_{h_1}}{dx} - \frac{du_s}{dx} \right) \Big|_A \delta_A \\ -\theta_f \left(\frac{du_{h_2}}{dx} - \frac{du_s}{dx} \right) \Big|_B + \frac{\theta_f}{\theta_s} f_s & \text{on } \Omega_g, \end{cases} \end{aligned} \quad (15)$$

where δ is the Dirac delta function and V is the functional space defined as

$$V = \left\{ (u_{h_1}, u_s, u_{h_2}) | u_{h_1} \in H^1(\Omega_{h_1}), u_s \in H^1(\Omega_s), u_{h_2} \in H^1(\Omega_{h_2}), u_s = u_{h_i} \text{ on } \partial\Omega_s, \theta_s \frac{du_s}{dx} = \theta_f \frac{du_{h_i}}{dx} \text{ on } \partial\Omega_s \right\}. \quad (16)$$

In Eq. (16), it can be observed that both the C^0 -continuity and the appropriate jump in the first derivative between the halo fluids and the solid are embedded in the function space V . In Eq. (15), note that the term $\frac{\theta_f}{\theta_s} f_s$ in the equation governing Problem 2 only has support on Ω_s . This term is added, in order to locally modify the global equation into the equation that describes the solid. Together with an extension of the forcing function, $f_f = 0$ on Ω_s , and the appropriate jumps in the derivative at the interfaces, this will force u_g to follow the solid solution u_s on the fictitious part of Ω_g . The appropriate jumps in the first derivative at the interfaces A and B are prescribed by the coefficients of the Dirac delta function in Eq. (15). As the global solution u_g equals both the solid solution u_s and the halo fluid solutions u_{h_1} and u_{h_2} on the corresponding intervals, it can be appreciated that the jump in first derivative of u_g can be prescribed by the jump in solid/halo fluid derivative across the interfaces A and B. Notice that these coefficients of the Dirac delta function, play the same role as the Lagrange multiplier in, for example Eq. (11). For more details about the implementation of the iterative solution method, we refer the reader to Maury [14].

In his work, Maury implemented the fat boundary method in a linear finite element framework to solve the two-dimensional Poisson problem in a domain with multiple voids. He successfully demonstrated the capabilities of the method and showed first order h -convergence.

5.2. Extension to higher order

Although in [3], an error estimate for the fat boundary method was given for p th order approximations, no results employing high-order methods have been published to our knowledge. In this section, we will show results for the fat boundary method implemented in a spectral/ hp element framework applied to the test problem introduced in Section 2. This corresponds to the solution of the weak equivalent of problem (15), solved using a spectral/ hp discretisation.

Fig. 10 shows the approximation error plotted as a function of the expansion order for a halo width of 0.3. An important observation can be made in this figure. Based on the discussion in Section 3.2, the global fluid approximation u_g which tries to describe first order discontinuities in the interior of elements, is expected to lead to non-exponential convergence. This is clearly visible in Fig. 10. However, it appears that this does not influence the convergence rate of the solid and halo fluid approximations. Furthermore, the part of the global fluid u_g that is of physical importance, i.e. the part of the fluid not described by the halo fluids, seems to converge exponentially. In Fig. 10, this part of the fluid is denoted as ‘Physical Fluid’. This means that the accuracy of the global approximation u_g is only locally affected by the jump in first derivative at the interfaces A and B. The numerical results show that, for our particular choice of grids and halo-size, the local unfavourable effect does not reach up to the outer points a and b , see Fig. 9, of the halo fluids. As in the fat Boundary method, the solid/halo fluid system (Problem 1) takes only information of the global problem (Problem 2) at points a and b , it can therefore be appreciated why both the solid and halo fluid approximation error converge exponentially. Apparently, the use of a halo mesh is not only advantageous for a better resolution of the approximation in the vicinity of the solid. In the context of high-order methods, the halo mesh can also be seen as a buffer

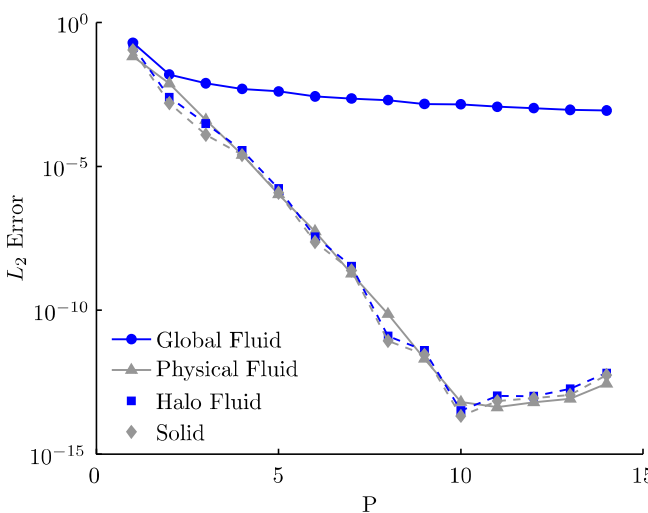


Fig. 10. p -Convergence of the fat boundary method applied to the 1D FSI test problem.

to local anomalies that allows for exponential error-convergence of the approximations.

However, from this point of view, it can be understood that the size of the halo mesh will be of importance. In Figs. 12–14, the error convergence is shown for three different halo-sizes. The different configurations are shown in Fig. 11.

Based on the results in these figures, it appears that it is the fact whether a global grid point is located inside the halo domain rather than the size of the halo, which is of major importance. These results demonstrate that exponential error-convergence will follow whenever a point of the global mesh is located inside the halo domain. Observing the results of cases 2 and 3 displayed in Figs. 13 and 14, respectively, it follows that the width of the halo mesh does not alter the results once this condition is fulfilled. On the

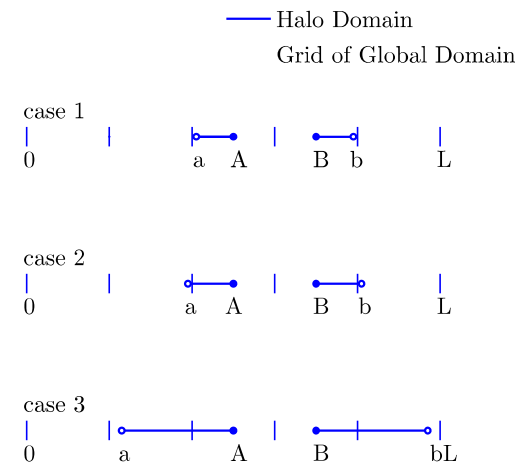


Fig. 11. The three different configurations of the halo boundary used to assess the convergence behaviour of the fat boundary method.

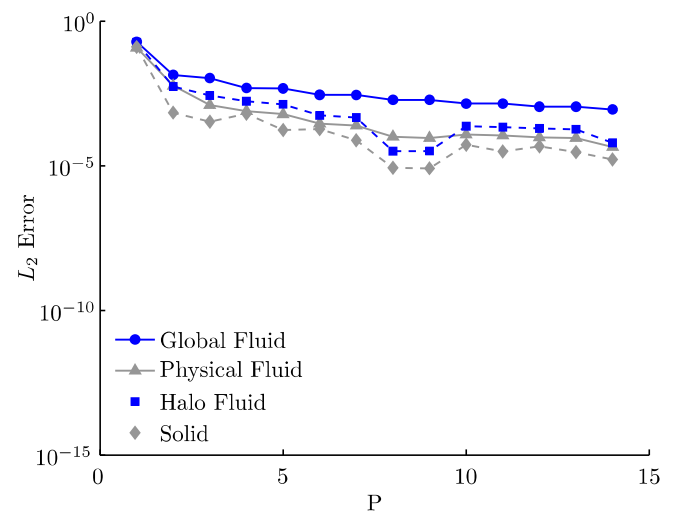


Fig. 12. p -Convergence of the fat boundary method applied to the 1D FSI test problem for case 2: the size of the halo boundaries is such that they just enclose an elemental interface of the global mesh.

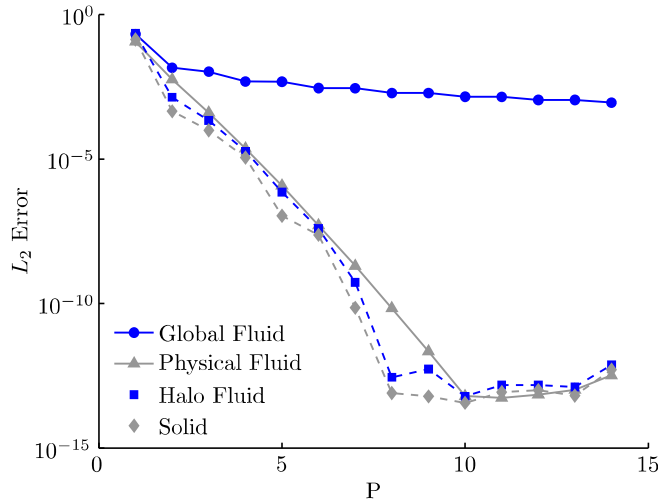


Fig. 13. p -Convergence of the fat boundary method applied to the 1D FSI test problem for case 2: the size of the halo boundaries is such that they just enclose an elemental interface of the global mesh.

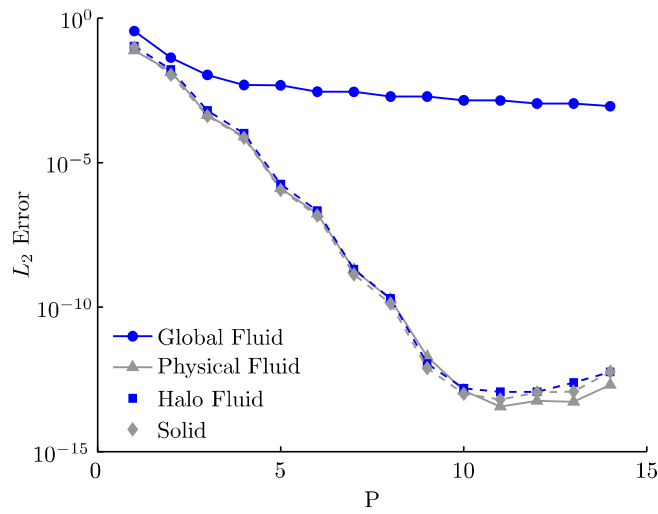


Fig. 14. p -convergence of the fat boundary method applied to the 1D FSI test problem for case 3: the size of the halo boundaries is such that they widely enclose an elemental interface of the global mesh.

other hand, when the halo domain is entirely embedded in single global element as for case 1, all approximations will be affected as demonstrated Fig. 12.

We observe that the local loss of accuracy of u_g is located around the physical interfaces A and B but does not pollute the global element boundaries. This observation is confirmed by Fig. 15, where the point-wise approximation error $(u_g - u_{ex})^2$ of the global solution is plotted as a function of the x -coordinate for a polynomial order $P = 8$ and employing six spectral/ hp elements. It can be seen that only in the global elements intersected by the physical interfaces, the point-wise error is inconsistent with the high-order spectral/ hp approximation. Hence, in order to get exponential p -convergence for the 1D test problem when using the fat boundary method, the following constraint should be satisfied:

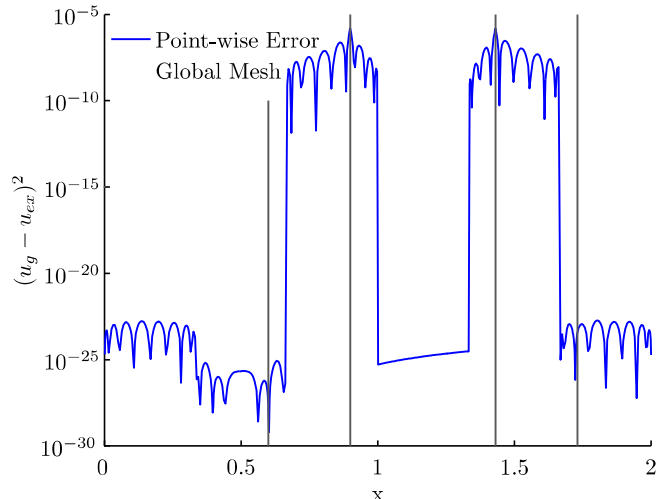


Fig. 15. Point-wise error of the fat boundary method with $P = 8$ applied to the 1D FSI test problem.

Constraint 5.1. The global background mesh and the halo domain should be chosen, such that the halo boundary encloses an elemental interface of the global domain.

This condition will always be satisfied if the halo mesh is chosen to be greater than the smallest segment of the discretised global domain.

5.3. Discussion

5.3.1. Implications of a halo boundary

The fat boundary method is mainly characterised by the introduction of a halo boundary. In the context of our extension to FSI problems, this implies that the solid body immersed in the fluid, is extended with a computational fluid domain. Employing a fine discretisation in the halo boundary, this will locally result in a high resolution of the fluid approximation. However, when the body is allowed to move throughout the fluid domain in a time-dependent problem, it can be appreciated that the halo boundary will cause problems if the solid body approaches other solid bodies or the edge of the computational domain. This makes the method unsuitable for problems in which solid bodies are expected to collide, as for example in the sedimentation of multiple particles suspended in a flow, which was successfully studied by Glowinski [10] using a DLM/FictD approach.

5.3.2. Extension to multiple dimensions

As shown in [14], the fat boundary method is suitable for two dimensional problems. However, in the context of an extension to the spectral/ hp element method, we have shown that for 1D test problem of Section 2, the mesh constraint 5.1 should be satisfied in order to benefit from exponential error-convergence. Our analysis would suggest that in multiple dimensions, a closed connection of C^0 -continuous edges of the global solution u_g should be enclosed in

the halo boundary at all times in order to guarantee exponential convergence. However, further investigation should be undertaken in order to validate this constraint in multiple dimensions.

5.3.3. Extension to other differential operators

For our 1D test problem of Section 2, a model based on Poisson equations is adopted. This allows the local modification of the global equation (the equation governing Problem 2 in Eq. (15)) on Ω_s into the solid equation employing the a priori known term $\frac{\partial f}{\partial s} f_s$. However, when considering problems governed by more complex PDE's, this local modification of the global equation might not be as straightforward and could possibly involve terms in terms of the variable u_s which will deteriorate the decoupling of the system.

Furthermore, an extension to other differential operators might possibly lead to a different behaviour of the point-wise error as observed in Fig. 15 which will affect the p -convergence of the fat boundary method. Also here, further investigation is required.

5.3.4. Implementation issues

The fat boundary method decouples the original problem into two sub-problems. As mentioned by Maury [14], Problem 2 governing the global solution u_g can be solved using fast solvers while the local sub-problems (Problem 1) can be solved fully parallel in the case of multiple particles. In addition, when considering time-dependent problems with moving objects, the stiffness-matrices of both sub-problems will remain invariant in time, which enhances the efficiency of the method.

6. An implicit fat boundary method

In this section, we will present an approach which combines the idea of an halo boundary, together with the use of Lagrange multipliers in a fictitious domain framework. We will refer to it as implicit fat boundary method. The proposed method is a variation of the fat boundary method proposed by Maury [14], which mainly differs from the original approach in the following respect:

- in order to get exponential convergence of u_g on every part of the global domain, we relax the condition that the global solution must approximate the physical solution in the fictitious domain and
 - a discrete Lagrange multiplier is employed to implicitly couple both sub-problems.

6.1. A modified global problem

It was discussed in Section 3.2, that the fictitious domain method exponentially converges when a mesh conforming to the physical interfaces is employed. This was related to the fact that the spectral/ hp element

method is capable of dealing with C^1 discontinuities if they are prescribed across element boundaries. If now, a halo fluid boundary is attached to the solid, the global fluid solution u_g does not have to represent the fluid solution on the halo domain anymore. In fact, u_g is only required to describe the physical fluid solution outside the region covered by the solid and surrounding halo fluid. As a consequence, introducing a halo boundary can be seen as an increase of the fictitious part of the global domain Ω_g . This implies that the kink in u_g , needed to connect the left and right solution in C^0 -continuous way, can be shifted into the halo domain. We then ensure that at least one grid point of the global mesh is located inside the halo boundary and impose the jump in first derivative at one of these particular grid point. Notice that this implies an identical constraint on the meshes as imposed to the original fat boundary method, see [constraint 5.1](#). This approach will turn out to be beneficial in a high-order context, as the spectral/ hp element can naturally deal with this kind of first order discontinuities.

For our one-dimensional test problem of Section 2, this will result in a configuration similar to that depicted in Fig. 9. In this figure, α and β denote the grid points of the global mesh at which the jump in first derivative will be imposed.

While the variables u_{h_i} and u_s , respectively represent the physical fluid and solid solutions in the corresponding domain, the following choices are made for the global solution u_g :

- in $[0, \alpha] \cup [\beta, L]$, u_g represents the physical fluid solution and
 - in $[\alpha, \beta]$, u_g represents a fictitious solution which is governed by the original fluid equation with a regular extension $f_f = \sin(\pi x)$ of the forcing function. Furthermore, this solution is C^0 -continuous to the solution outside this domain.

This problem can be formulated as: find $\{u_f, (u_{h_1}, u_s, u_{h_2})\} \in H_0^1(\Omega_g) \times V$ such that,

$$\text{Problem 1 : } \begin{cases} \frac{d}{dx} \left(\theta_f \frac{du_{h_2}}{dx} \right) = f_f & \text{on } \Omega_{h_1} \\ \frac{d}{dx} \left(\theta_s \frac{du_s}{dx} \right) = f_s & \text{on } \Omega_s \\ \frac{d}{dx} \left(\theta_f \frac{du_{h_2}}{dx} \right) = f_f & \text{on } \Omega_{h_2} \end{cases} \quad (17)$$

$$\text{Problem 2 : } \left\{ \begin{array}{l} \frac{d}{dx} \left(\theta_f \frac{du_f}{dx} \right) = f_f = \sin(\pi x) \\ \text{on } [0, \alpha] \cup [\alpha, \beta] \cup [\beta, L], \end{array} \right. \quad (18)$$

subject to the constraints:

$$\theta_f \frac{du_g}{dx} \Big|_a = \theta_f \frac{du_{h1}}{dx} \Big|_a, \quad \theta_f \frac{du_g}{dx} \Big|_b = \theta_f \frac{du_{h2}}{dx} \Big|_b, \quad (19)$$

$$u_g|_{\alpha} = u_{h_1}|_{\alpha} \quad , \quad u_g|_{\beta} = u_{h_2}|_{\beta}, \quad (20)$$

where V is the function as defined in Eq. (16). This latter set of constraints couples both sub-problems. For the 1D

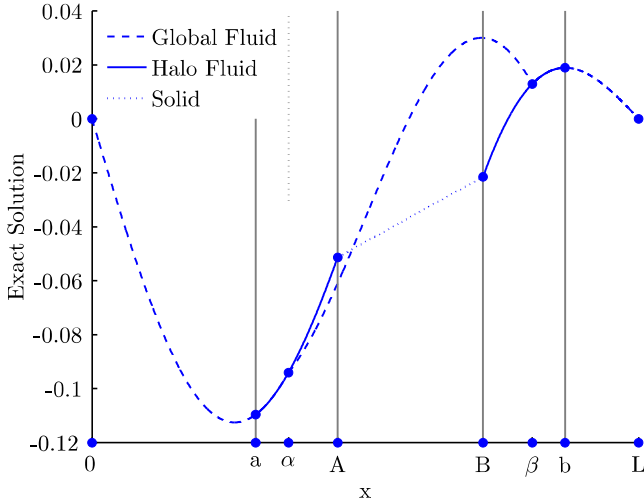


Fig. 16. Exact solution of the different variables of the implicit fat boundary method applied to the 1D FSI test problem.

fluid–structure interaction test problem, the exact solution of the modified fat boundary method is shown in Fig. 16. The jumps in first derivative at the points α and β are clearly visible in this picture.

6.2. Introduction of a discrete Lagrange multiplier

A discrete Lagrange multiplier will be applied at the points α and β in order to impose constraint (20). Following a procedure as proposed by Yu [20] for the DLM/FictD method (see also Section 3.1), we would expect the following weak formulation:

Find $\{u_f, (u_{h_1}, u_s, u_{h_2}), \lambda_{\alpha, \beta}\} \in H_0^1(\Omega_g) \times V \times \mathbb{R}$ such that

$$\int_0^L \theta_f \frac{dv_f}{dx} \frac{du_g}{dx} dx + \lambda_\beta v_f(\beta) - \lambda_\alpha v_f(\alpha) = - \int_0^L v_f f_f dx \quad \forall v_f, \quad (21)$$

$$\int_a^A \theta_f \frac{dv_{h_1}}{dx} \frac{du_{h_1}}{dx} dx - \int_a^A \theta_f \frac{dv_{h_1}}{dx} \frac{du_g}{dx} dx + \lambda_\alpha v_{h_1}(\alpha) = 0 \quad \forall v_{h_1}, \quad (22)$$

$$\int_A^B \theta_s \frac{dv_s}{dx} \frac{du_s}{dx} dx - \int_A^B \theta_f \frac{dv_s}{dx} \frac{du_g}{dx} dx = - \int_A^B v_s (f_s - f_f) dx \quad \forall v_s, \quad (23)$$

$$\int_B^b \theta_f \frac{dv_{h_2}}{dx} \frac{du_{h_2}}{dx} dx - \int_B^b \theta_f \frac{dv_{h_2}}{dx} \frac{du_g}{dx} dx - \lambda_\beta v_{h_2}(\beta) = 0 \quad \forall v_{h_2}, \quad (24)$$

$$\gamma_\alpha (u_g - u_{h_1})|_{x=\alpha} = 0 \quad \forall \gamma_\alpha, \quad (25)$$

$$\gamma_\beta (u_g - u_{h_2})|_{x=\beta} = 0 \quad \forall \gamma_\beta. \quad (26)$$

However, starting from the strong formulation Eqs. (17)–(20) and applying variational calculus, another weak formulation can be derived:

Find $\{u_f, (u_{h_1}, u_s, u_{h_2}), \lambda_{\alpha, \beta}\} \in H_0^1(\Omega_g) \times V \times \mathbb{R}$ such that,

$$\int_0^L \theta_f \frac{dv_f}{dx} \frac{du_g}{dx} dx + \lambda_\beta v_f(\beta) - \lambda_\alpha v_f(\alpha) = - \int_0^L v_f f_f dx \quad \forall v_f, \quad (27)$$

$$\int_a^A \theta_f \frac{dv_{h_1}}{dx} \frac{du_{h_1}}{dx} dx + \theta_f \frac{du_g}{dx} \Big|_a v_{h_1}(a) = - \int_a^A v_{h_1} f_{h_1} dx \quad \forall v_{h_1}, \quad (28)$$

$$\int_A^B \theta_s \frac{dv_s}{dx} \frac{du_s}{dx} dx = - \int_A^B v_s f_s dx \quad \forall v_s, \quad (29)$$

$$\int_B^b \theta_f \frac{dv_{h_2}}{dx} \frac{du_{h_2}}{dx} dx - \theta_f \frac{du_g}{dx} \Big|_b v_{h_2}(b) = - \int_a^A v_{h_2} f_{h_2} dx \quad \forall v_{h_2}, \quad (30)$$

$$\gamma_\alpha (u_g - u_{h_1})|_{x=\alpha} = 0 \quad \forall \gamma_\alpha, \quad (31)$$

$$\gamma_\beta (u_g - u_{h_2})|_{x=\beta} = 0 \quad \forall \gamma_\beta. \quad (32)$$

Although both formulations are equivalent, they involve different terms. Notice that for the first formulation, the global fluid equation, Eq. (21), is subtracted from Eqs. (22)–(24). A similar observation could be made for the DLM/FictD formulation given by Eqs. (7) and (8). Evaluating these resulting weak equations using integration by parts, it can be appreciated that these terms are only there to enforce the appropriate boundary conditions of the local problems. However, as in the case of the modified fat boundary method, the boundary conditions at the outer edges of the local problem are explicitly given by Eq. (19), they can be inserted in the weak formulation in order to replace the integral terms. This results in the formulation given by Eqs. (27)–(32).

Even though both weak systems are completely equivalent, the new off-diagonal coupling terms in Eqs. (28)–(30) are considerably easier to evaluate than the integral terms appearing in Eqs. (22)–(24), in particular because the integrands will be non-smooth due to the jump in the first derivative of u_g at the points α and β . As discussed in Section 4.3.2, this kind of integrals might be very cumbersome to evaluate in multiple dimensions. The fact that these integrals can be eliminated, enhances the efficiency of the proposed method. However, note that the first formulation Eqs. (21)–(26) is symmetric, while the second Eqs. (27)–(32) is not.

6.3. Numerical results

To evaluate the proposed variation of the fat boundary method, the 1D FSI problem of Section 2 is solved using a spectral/ hp element discretisation. In Fig. 17, it can be observed that the proposed method does convergence

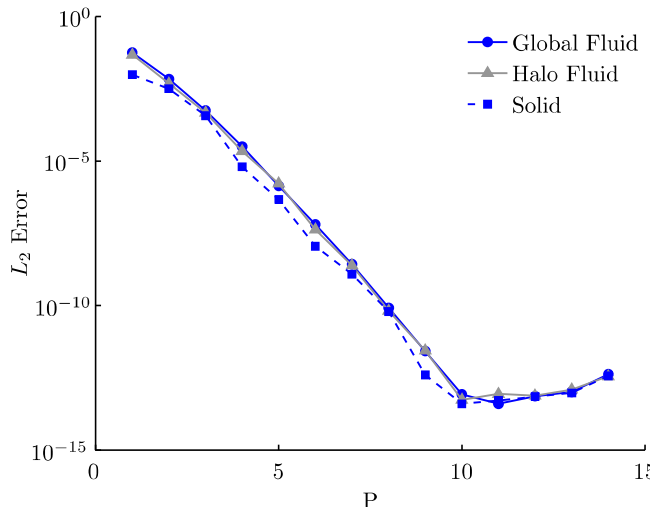


Fig. 17. Exponential p -convergence of the implicit fat boundary method applied to the 1D FSI test problem.

exponentially for the test problem of Section 2. As opposed to the original fat boundary method, the error of the global solution u_g now converges exponentially on its entire domain. In Fig. 17, the error of the global fluid is defined as the error of u_g on the interval $[0, L]$, taking into account the error of the fictitious part of the solution.

6.4. Discussion

6.4.1. Implications of the modified global problem

While for the original fat boundary method, Constraint 5.1 introduced in Section 5.2 was just a condition for high-order convergence for the 1D test problem, it is an absolute constraint for the applicability of the modified fat boundary method. If the relation between the halo domain and the global mesh does not satisfy the constraint, the modified fat boundary method will be ill-posed. However, as a suitable implementation of the method proposed in this section will always lead to exponential error-convergence when approximating smooth solutions, the implicit fat boundary method can be classified as a real high-order method to solve fluid–structure interaction problems.

In the original fat boundary method, it was required that the global fluid equation could be locally modified into the solid as discussed in Section 5.3.3. Due to the relaxation of this constraint, such a condition should not hold for the implicit fat boundary method. In addition, while the original FBM relies on the fact that the global approximation is only locally polluted as observed in Fig. 15, the convergence rate of the implicit fat boundary method is not based on such a condition. Both these observations make the implicit FBM suitable for solving problems governed by equations other than the Poisson equation.

Further, due to the presence of a halo boundary around the solids, this approach will not be applicable in the case of problems involving colliding objects.

Finally, we would like to mention that when the Lagrange multipliers in the implicit FBM will be imposed on the points A and B rather than the global grid points α and β , the proposed fat boundary method can be seen as the implicit variant of the original boundary method. However, note that the points were the Neumann and Dirichlet boundary conditions are imposed on the different sub-problems have been swapped around compared to the original FBM. This implicit variant will not exhibit exponential convergence of the global approximation on its entire domain, as observed in the original FBM.

6.4.2. Extension to multiple dimensions

With respect to the constraint imposed to the proposed method, the same arguments as discussed in Section 5.3.2 apply for the implicit FBM method.

Furthermore, we would like to reiterate that, in a context of multiple dimensions, the elimination of the off-diagonal terms in the system governed by Eqs. (21)–(26), can be considered as very favourable.

6.4.3. Implementation issues

As the governing fluid equation is extended into the fictitious domain, the stiffness matrix of the global problem will remain invariant in time for unsteady simulations. In addition, due to the regular extension of the forcing function $f_f = \sin(\pi x)$ into the fictitious domain, also the right hand side vector will remain invariant. This means that all diagonal blocks in the resulting global matrix will be fixed, and hence, need only to be calculated once. Only the off-diagonal blocks, which mutually couple the different sub-problems, will need to be recalculated when the solid object is moving throughout the solid domain. But as these off-diagonal terms only consists of algebraic expressions, as can be seen in Eqs. (27)–(32), this will be a relatively efficient process.

7. Conclusion

Different methods using fictitious domains have been analysed in the context of spectral/ hp elements discretisations. The methods considered were taken from the existing literature and have been extended/adapted where necessary to fit our generalised test problem, i.e. a fluid with an immersed solid, both described by the Poisson equation, but with different coefficients and forcing functions. The Poisson models on a 1D domain allow us to focus on the similarities and differences between the proposed methods in an clear and organised manner.

We considered the following approaches:

- The fictitious domain method [10,6].
- The finite cell method [15].
- The fat boundary method [14,3].
- The implicit fat boundary method (proposed in this paper).

Different model problems can be distinguished based on four definitions for the structural part, being: (1) voids, (2) rigid bodies (a priori known position/rotation), (3) rigid bodies (a priori unknown position/rotation) and (4) deformable bodies. Depending on the type of structural body, the boundary conditions will be different and formulations will change. None of the above approaches considered model problems with deformable bodies (i.e. described by a PDE) in a spectral/ hp element context. In order to address this most general model problem, an extension to the finite cell and fat boundary method have been proposed. Furthermore, an alternative Lagrange multiplier based variation on the fat boundary method was introduced, which we named the implicit fat boundary method to discriminate both methods. The accuracy of the methods was investigated through p -convergence plots of the L_2 error defined by Eq. (5).

The first method considered is the fictitious domain method as employed by Glowinski et al. [10] using finite elements and explored by Dong et al. [6] using spectral/ hp elements (Section 3). For a solid–fluid interaction problem the global fluid is forced to follow the solid solution across the total fictitious part of the domain by means of distributed Lagrange multipliers. For our test problem no exponential p -convergence is obtained. The reason is that a jump in the first derivative will occur inside an element of the global fluid mesh which can not be correctly resolved by the (high-order) polynomials due to lack of smoothness. Although the solution seems to approximate the exact solution reasonably well, the lack of convergence indicates that this approach does not fully benefit from the advantages of the spectral/ hp approach.

The second method explored is the finite cell method (Section 4) by Parvizian et al. [15]. Their approach diminishes the contribution of the fictitious part of the global fluid to the total solution by pre-multiplying the PDE by a parameter $\theta \ll 1$ in this part of the domain. This makes the method similar to a penalty method. Parvizian et al. already demonstrated an exponential p -convergence of the method in the case of voids and the introduction of a solid PDE in the fictitious domain in this work extends this beneficial behaviour of the method to a more general case. The major disadvantage of the method is that the global matrix will become more ill-posed with an increasing polynomial order due to canceling part of the interface integrals. And because the method involves the evaluation of integrals with discontinuous integrands across the physical interface, its accuracy might be adversely influenced by integration errors.

The third approach taken from literature is the fat boundary method [14], which considers a boundary layer of fluid around an object (Section 5). In a Neumann–Dirichlet fixed point iteration scheme boundary conditions are imposed in an alternating manner at respectively the inner and outer boundary of the boundary fluid. In this work objects are considered that contain an analytically known solution and the convergence of the method is dem-

onstrated for a first order finite element code. We implemented the fat boundary method in a spectral/ hp framework and demonstrated exponential p -convergence as predicted [3]. The only mesh requirement was that the halo boundary should enclose at least one point of the global fluid mesh. A downside of the approach is that contact between multiple solid bodies (e.g. particle sedimentation) will introduce problems, although this problem is neither trivial for the finite cell method.

An new alternative approach, the implicit fat boundary method, was proposed (Section 6) that is a combination of the classic fictitious domain method and the fat boundary method. Similar to the fat boundary method a fluid layer aligning the object is introduced, but both sub-problems are implicitly coupled using a discrete Lagrange multiplier. The method is characterised by convergence of the fictitious global fluid solution which is not forced to approximate the underlying solid solution. The same mesh requirement as for the fat boundary holds, i.e. one point of the global fluid mesh must lie within the halo boundary fluid and at that point the constraints should be applied. An exponential p -convergence was demonstrated when this requirement is met.

Although the 1D Poisson model provides a good framework to gain knowledge on the behaviour of jumps of coefficients, forcing functions and first derivatives or on the use of Lagrange multipliers, an implementation in 2D or 3D will obviously introduce additional issues. Exact integration at the interface will become a serious issue as addressed in many other papers. Adaptive mesh refinement (quadtree) for the integrals or higher order integration (overintegration) have been suggested as alternative strategies to exact integration. How these integration issues will influence the convergence behaviour for the different methods in a higher order context, will certainly be of interest for future research. Furthermore, the separate halo domains in our 1D example will become a single domain if the problem is extended to a structure with a halo fluid. As a consequence the discontinuities in the first derivatives will occur across a curve rather than a point. This will influence the sensitivity of the method with regard to the mapping of solutions between domains as is well known. Adopting a model using the Poisson equation is of course another simplification which has its limitations.

Finally, the aim of this work was not only to demonstrate the performance of methods using fictitious domains in a spectral/ hp framework, but also to provide insight in the behaviour of non-matching methods in general. This can be useful in any finite element formulation for making compromises between accuracy and complexity depending on the application.

Acknowledgements

The first and last author would like to acknowledge support from an EPSRC Advanced Research Fellowship. The second author is funded by “Human Resources and

Mobility" within the sixth framework program by means of a Marie Curie Intra-European Fellowship. The authors would also like to thank F.P.T Baaijens for the inspiration.

References

- [1] F.P. T Baaijens, A fictitious domain/mortar element method for fluid–structure interaction, *Int. J. Num. Meth. Fluids* 35 (7) (2001) 743–761.
- [2] F. Bertrand, P.A. Tanguy, F. Thibault, A three-dimensional fictitious domain method for incompressible fluid flow problems, *Int. J. Num. Meth. Fluids* 25 (6) (1997) 719–736.
- [3] S. Bertoluzza, M. Ismail, B. Maury, The fat boundary method: semi-discrete scheme and some numerical experiments, *Domain Decompos. Meth. Sci. Engrg.* 40 (2005) 513–520.
- [4] R.P. Beyer, R.J. Leveque, Analysis of a one-dimensional model for the immersed boundary method, *SIAM J. Numer. Anal.* 29 (2) (1992) 332–364.
- [5] A. de Boer, A.H. van Zuijlen, H. Bijl, Review of coupling methods for non-matching meshes, *Comp. Meth. Appl. Mech. Engrg.* 196 (2007) 1515–1525.
- [6] S. Dong, D. Liu, M.R. Maxey, G.E. Karniadakis, Spectral distributed Lagrange multiplier method: algorithm and benchmark tests, *J. Comp. Phys.* 195 (2004) 695–717.
- [7] A. Gilmanov, F. Sotiropoulos, A hybrid Cartesian/immersed boundary method for simulating flows with 3d, geometrically complex, moving bodies, *J. Comp. Phys.* 207 (2005) 457–492.
- [8] R. Glowinski, T.-W. Pan, J. Périoux, A fictitious domain method for Dirichlet problem and applications, *Comp. Meth. Appl. Mech. Engrg.* 111 (1994) 283–303.
- [9] R. Glowinski, T.-W. Pan, J. Périoux, A Lagrange multiplier/fictitious domain method for the numerical simulation of incompressible viscous flow around moving rigid bodies: (i) case where the rigid body motions are known a priori, *C.R. Acad. Sci. Paris* 25 (5) (1997) 361–369.
- [10] R. Glowinski, T.-W. Pan, T.I. Hesla, D.D. Joseph, A distributed Lagrange multiplier/fictitious domain method for particulate flows, *Int. J. Multiphase Flow* 25 (1997) 755–794.
- [11] W.R. Hwang, M.A. Hulsen, H.E.H. Meijer, Direct simulation of particle suspensions in sliding bi-periodic frames, *J. Comp. Phys.* 194 (2004) 742–772.
- [12] G.E. Karniadakis, S.J. Sherwin, *Spectral/hp Element Methods for Computational Fluid Dynamics*, Oxford Science Publications, 2005.
- [13] R.J. Leveque, Z. Li, Immersed interface methods for Stokes flow with elastic boundaries or surface tension, *SIAM J. Sci. Comput.* 18 (1997) 709–735.
- [14] B. Maury, A fat boundary method for the poisson problem in a domain with holes, *J. Sci. Comput.* 16 (3) (2001) 319–339.
- [15] J. Parvizian, A. Düster, E. Rank, Finite cell method, *Comput. Mech.*, doi:10.1007/s00466-007-0173-y, 2007.
- [16] C.S. Peskin, The immersed boundary method, *Acta Numerica* 11 (2002) 479–517.
- [17] R. Van Loon, P.D. Anderson, F.N. Van de Vosse, S.J. Sherwin, Comparison of various fluid–structure interaction methods for deformable bodies, *Comp. Struct.* 85 (2006) 833–843.
- [18] X. Wang, From immersed boundary method to immersed continuum method, *Int. J. Multiscale Comp. Engrg.* 4 (2006) 127–145.
- [19] X. Wang, W.K. Liu, Extended immersed boundary method using FEM and RKPM, *Comput. Meth. Appl. Mech. Engrg.* 193 (2004) 1305–1321.
- [20] Z. Yu, A DLM/FD method for fluid/flexible-body interactions, *J. Comp. Phys.* 207 (2005) 1–27.
- [21] L. Zhang, A. Gerstenberger, X. Wang, W.K. Liu, Immersed finite element method, *Comput. Meth. Appl. Mech. Engrg.* 193 (2004) 2015–2067.